Soft Matter

ARTICLE TYPE

Cite this: DOI: 00.0000/xxxxxxxxxx

Self-assembly behavior of experimentally realizable lobed patchy particles[†]

Sanjib Paula and Harish Vashisth *a

Received Date Accepted Date

11

13

17

19

20

22

23

24

27

29

30

DOI: 00.0000/xxxxxxxxxx

We report simulation studies on the self-assembly behavior of five different types of lobed patchy particles of different 34 shapes (snowman, dumbbell, trigonal planar, square planar, and tetrahedral). Inspired by an experimental method of synthesizing patchy particles (Wang et al., Nature, 2012, 491:51-55), we control the lobe size indirectly by gradually varying the seed diameter and study its effect on self-assembled structures at different temperatures. Snowman shaped particles self-assemble only at a lower temperature and form two-dimensional sheets, elongated micelles, and spherical micelles, depending on the seed diameter. Each of the four other lobed particles self-assemble into four distinct morphologies (random aggregates, spherical aggregates, liquid droplets, and crystalline structures) for a given lobe size and temperature. We observed temperature-dependent transitions between two morphologies depending on the type of the lobed particle. The self-assembled structures formed by these four types of particles are porous. We show that their porosities can be tuned by controlling the lobe size and temperature.

Self-assembly of colloidal patchy particles is an emerging and solution novel way of obtaining unique morphologies for various technological and biomedical applications 1–6. Guided by the site-specific directional interactions, these particles have the potential to self-assemble into higher order structures (for example, chains 7, two-dimensional sheets 7, and even more complex structures like a diamond crystal 8) which cannot be obtained by other synthetic routes. Because of their unparalleled importance, recent years have witnessed an effort, both in theory and experiments, in designing patchy particles, and studying their self-assembly behavior 9–22. Among key factors that control the phases and the morphologies of self-assembled structures are the size of the

patches, interaction strength between the patches, temperature and volume fraction of particles along with the intrinsic factors like the number and the location of patches.

In a recent work 23, spherical Janus particles, which interacted through DNA functionalized attractive patches, were found to self-assemble into diverse structures (colloidal micelles, chains and bilayers) depending on the patch size. Patch size is a critical property that rules the self-assembly of particles into desired structures. While larger patches allow more flexibility and thus lead to misassembly, smaller patches are more likely to produce targeted structures 24,25. Liu et al. 26 showed that the dumbbell shaped Au-Fe₃O₄ nanocrystals comprised of two spherical beads (the particles having two spherical beads are called snowman shaped particles in the present study), in which one bead is attractive and another one is repulsive, self-assemble into different superstructures (dimers, trimers, tetramers) at different bead size ratios. Wang et al. 11 reported a method of making non-spherical patchy particles, where patches around a central spherical seed appear as protrusions or lobes, and showed a way of getting different self-assembled structures by controlling the patch size. Using the emulsion and evaporation technique ²⁷, they first made clusters of different shapes (spheres, dumbbells, triangles, tetrahedral, triangular bipyramidal, octahedral, and pentagonal bipyramidal) which were comprised of n (n varies from 1 to 7) number of amidinated polystyrene beads. In the next step, the clusters were swelled and polymerized using the styrene monomers. The exposed parts of polystyrene beads, after the swelling and polymerization are done, appear as protrusions or lobes and act as patches. Patch sizes were observed to depend entirely on the extent of swelling. Higher is the swelling, lower is the patch size and vice-versa. The amidinated patches can be subjected to further functionalization by molecules like complementary DNA strands or pilandromes to induce directional interactions between the particles. The patchy particles thus produced self-assemble and generate different morphological structures depending upon their patch sizes. For example, particles having two patches on two opposite sides of the central seed self-

^a Department of Chemical Engineering, University of New Hampshire, 33 Academic 67 Way, Durham, NH 03824, USA; E-mail: harish.vashisth@unh.edu

[†] Electronic Supplementary Information (ESI) available: Ten figures (modeling of snowman shaped particles, simulation domains, radial distribution functions, and ⁶⁹ pore size distributions) are included in the ESI.

assemble into linear chains, when the patch size is smaller. But when patches are made bigger, the same particles were observed to form branched chains.

72

73

74

76

77

78

79

80

81

82

83

84

87

89

90

92

93

95

96

97

98

99

100

101

102

103

104

105

106

107

108

109

110

111

112

113

114

115

116

117

118

119

120

121

122

123

124

125

126

In our previous work ²⁸, we studied the self-assembly of seven different types of lobed particles (snowman, dumbbell, trigonal planar, square planar, tetrahedral, trigonal bipyramidal, and octahedral). We kept the seed to lobe diameter ratio constant and varied the attractive interactions between the lobes to understand its effect on the self-assembly. The self-assembled structures generated by these particles (except snowman) were found to be either porous amorphous or porous crystalline. A porous selfassembled structure could find many applications, for example, in tissue engineering, if the pore diameters are in the micron scale range ^{29,30}. The dumbbell, trigonal planar, and square planar particles were observed to generate highly porous structures compared to the other three types of particles (tetrahedral, trigonal bipyramidal, and octahedral)²⁸. The self-assembled morphologies and the porosities were found to be independent of a range of volume fractions of the lobed particles.

In the present work, we extended our previous study, and investigated in detail the effect of lobe size on the self-assembled morphologies and porosities for five different particles (snowman, dumbbell, trigonal planar, square planar, and tetrahedral). Except the square planar particles, the other four types of particles are experimentally realizable 11,31-33. The square planar lobed particles are analogues of the square planar patchy particles (having four surface patches at four equatorial positions) studied by Zhang et al⁷. The inclusion of square planar particles in the present study allows to examine the effect of shapes on the self-assembled structures formed by two different types 127 of particles having the same number of lobes (square planar and tetrahedral). To model the lobed particles, we followed an approach inspired by the work of Pine and coworkers 11. We have not chosen trigonal bipyramidal and octahedral lobed particles in this study, as these two types of particles are not promising, 132 to produce highly porous structures, as revealed by our previous 133 work 28 . Moreover, the porosities generated by these two types of $_{_{134}}$ particles were found to be comparable with the tetrahedral lobed $_{_{135}}$ particles and therefore, in this work, we choose to study only the tetrahedral particles among the tetrahedral, trigonal bipyramidal, and octahedral lobed particles.

Specifically, we studied the self-assembly of five different types 198 of particles: (i) snowman, (ii) dumbbell, (iii) trigonal planar, (iv) 140 square planar, and (v) tetrahedral. The particles are different 141 in terms of their shapes (Fig. 1 and Fig. S1) and the number 142 of lobes attached to the seed. To understand the effect of lobe 143 size on self-assembled morphologies, we modeled our particles to 144 closely resemble the experimental method of synthesizing patchy 145 lobed particles, as proposed by Pine and co-workers 11. To mimic 146 the experimental protocol for particle design, we first make clusters of spherical particles, and then grow the central repulsive 148 spheres from the centers of mass of these clusters. We term these 149 central repulsive spheres as seeds in this work complying with 150 our previous work on these lobed particles 28. However, from an 151 experimental point of view, seeds are usually referred to the initial spheres where a second stage reaction is carried out to grow 153

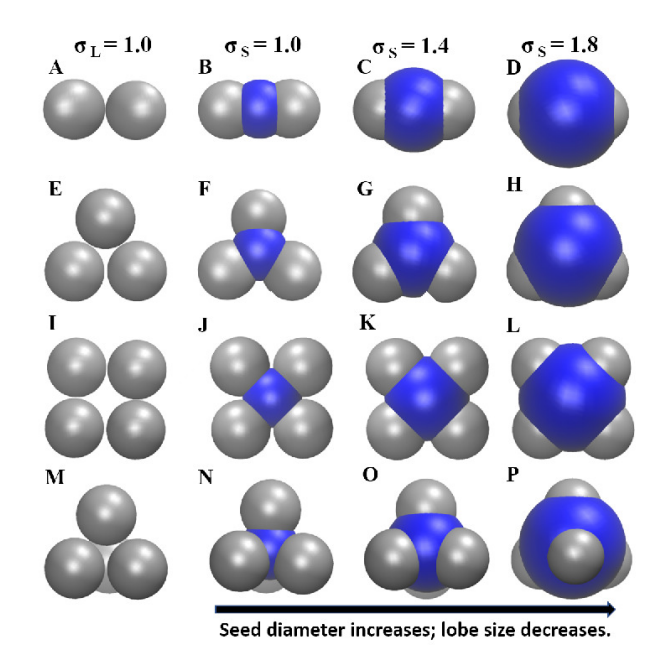


Fig. 1 A pictorial representation of changing the lobe (gray) size by controlling the seed (blue) diameter for dumbbell (A-D), trigonal planar (E-H), square planar (I-L), and tetrahedral (M-P) shaped lobed particles. The clusters of spherical beads of diameter σ_L =1.0 are shown in the first column (A, E, I and M). The seed diameter was gradually increased from σ_S = 1.0 to 2.0. We show lobed particles only for three seed diameters (σ_S): 1.0 (second column), 1.4 (third column), and 1.8 (fourth column). For the snowman shaped particles, we follow a different way to vary the lobe size (Fig. S1, ESI†).

lobes. In the case of tetrahedral lobed particles, for example, we first created a uniform tetrahedral cluster using four spherical beads (Fig. 1M). Then, we placed the seed at the center of mass of the cluster. The exposed parts of spherical beads that remain after inserting the seed become lobes. We gradually increase the diameter of the seed to control the lobe size (Fig. 1N-P). A higher seed diameter leads to a smaller lobe size. We follow the same approach for all lobed particles except for the snowman shaped particles because these particles have only one lobe. Therefore, it is not meaningful to make a cluster using one spherical bead and inserting the seed at the center of mass of the cluster. In that case, we placed a lobe and a seed (two spherical beads) at a $0.5~\sigma_L$ (σ_L is the diameter of the spherical beads and the distance units are used in all simulations) apart and varied the seed diameter to obtain different lobe sizes (Fig. S1, ESI †).

We carried out Langevin molecular dynamics simulations in dimensionless units using the HOOMD-Blue software 34,35 . The diameters of spherical beads that constitute the initial cluster follow distance units ($\sigma_L = 1.0$). We gradually increase the seed diameter starting from 1.0 to 2.0 ($\sigma_S = 1.0, 1.2, 1.4, 1.6, 1.8, 2.0$). We define a dimensionless parameter, q, which is the ratio of the diameter of spherical beads forming the initial clusters to the diameter of the central seed, $q = \sigma_L/\sigma_S$. As we increase the seed diameter from 1.0 to 2.0, the values of q decreases from 1.0 to 0.5 (q = 1.0, 0.83, 0.71, 0.63, 0.56, 0.50) with a decrease in the lobe size. The masses of lobes and seeds are held constant and equal to 1.0 ($m_S = m_L = 1.0$).

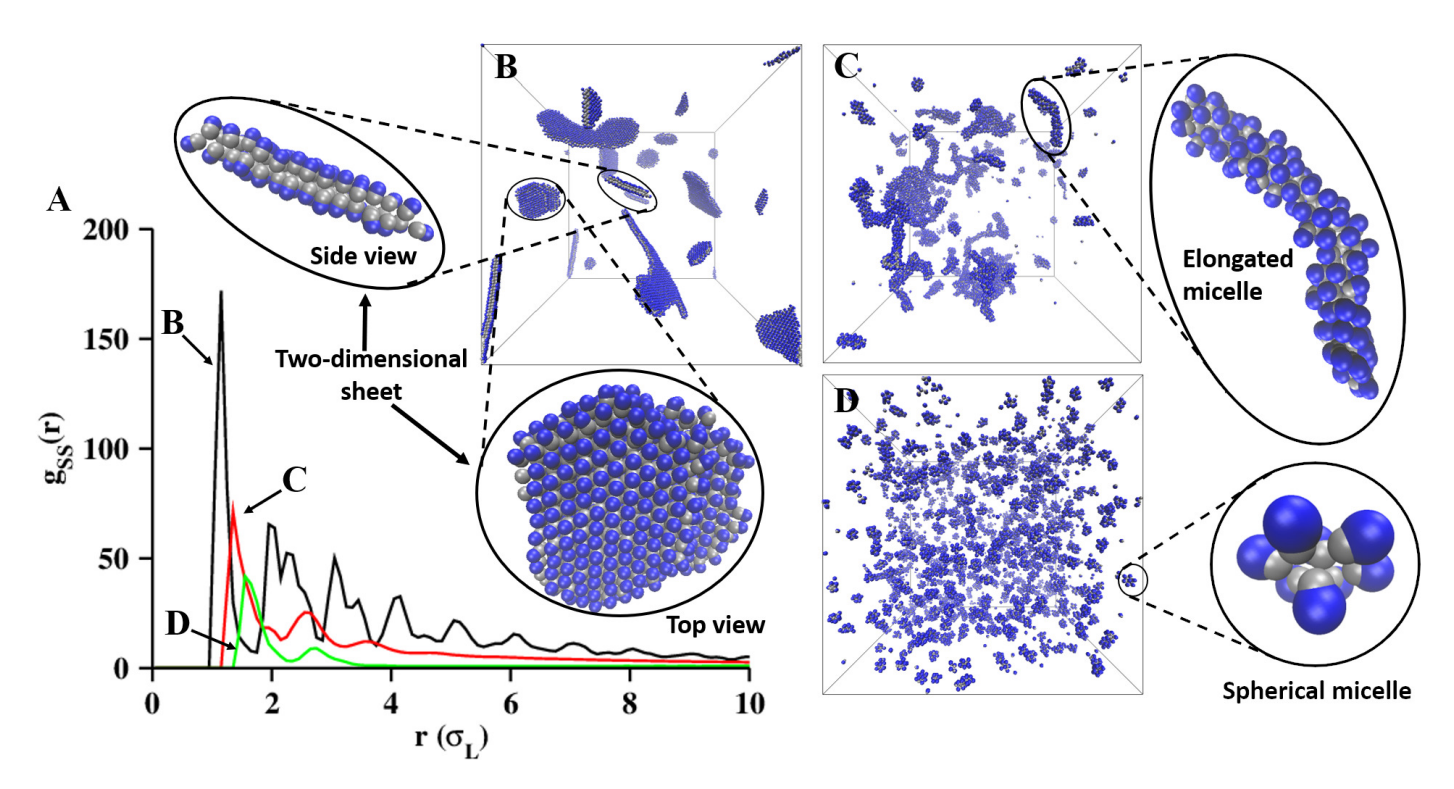


Fig. 2 Self-assembly of snowman shaped particles at different seed diameters. (A) Radial distribution functions [$g_{SS}(r)$] computed for the seed pairs at $k_BT=0.2$ at three different seed diameters: $\sigma_S=1.0$ (B), 1.2 (C) and 1.4 (D). Shown are simulation domains with (B) 2D sheets at $k_BT=0.2$ and $\sigma_S=1.0$; the enlarged side and top views of these sheets are shown separately, (C) elongated micelles at $k_BT=0.2$ and $\sigma_S=1.2$, and (D) spherical micelles at $k_BT=0.2$ and $\sigma_S=1.4$.

All types of non-bonded interactions (lobe-lobe, seed-seed, 182 and seed-lobe) between the particles are modeled by a sur-183 face shifted Lennard-Jones (SSLJ) potential (see supplemental 184 methods, ESI †). We studied the effect of temperature on self-185 assembled morphologies and their porosities. We randomized 186 the initial configurations by simulating each system at a higher 187 temperature ($k_BT=1.8$) before simulating the self-assembly at 188 other temperatures. We investigated a wide range of tempera-189 tures starting from 0.2 to 1.2 ($k_BT=0.2, 0.4, 0.6, 0.8, 1.0, 1.2$). 190 The inter-lobe interactions employed in this work ($\varepsilon_{LL}=1.0; \varepsilon_{LL}$ 191 is the well depth in the SSLJ potential for the lobe-lobe pairs) 192 vary from 0.83 k_BT (at $k_BT=1.2$) to 5 k_BT (at $k_BT=0.2$), which 193 is experimentally realizable. In a recent work, Tsyrenova et al. 19 194 reported on how the van der Waals attractions between metal 195 coated patches can be altered by changing the thickness of the 196 metal.

154

155

156

157

158

159

160

161

162

163

164

165

166

167

168

169

170

171

172

173

174

175

176

177

178

179

180

181

Depending on the number of lobes, the lobe size, and the tem-198 perature, we observed that lobed patchy particles self-assemble 199 into different morphologies. We calculated radial distribu-200 tion functions (RDFs) to understand the morphologies of self-201 assembled structures and also to distinguish between different 202 structures generated at different seed diameters and tempera-203 tures (see supplemental methods, ESI†). We also report the 204 change in the potential energy per particle with time to exam-205 ine the stability of self-assembled structures (Fig. S2, ESI†). Here,206 we report equilibrium morphologies and porosities obtained from 207 self-assembled structures at the end of each simulation.

Self-assembled morphologies: Snowman shaped particles209

show self-assembly only at a very low temperature ($k_BT = 0.2$) and are observed to generate three different morphologies at three different seed diameters, $\sigma_S = 1.0$ (q = 1.0), 1.2 (q = 0.83), and 1.4 (q = 0.71). At $\sigma_S = 1.0$, these particles self-assemble into two layers to form two-dimensional sheet like structures (Fig. 2B). In the two layers of these sheets, lobes remain buried and seeds remain exposed to the solvent. The RDFs computed for the seed pairs shows multiple peaks at a regular interval (Fig. 2A), indicating the presence of highly correlated and ordered particles. The two-dimensional sheets were found to be disassembled at a higher temperature, as we examined its stability by simulating the low-temperature structures at a higher temperature ($k_BT = 0.4$). When the seed diameter is increased to 1.2, snowman particles assemble into elongated micelles (Fig. 2C), and into spherical micelles (Fig. 2D) at a seed diameter of 1.4. If the seed diameter is increased beyond 1.4, snowman particles do not self-assemble at any of the temperatures employed in this work. This occurs due to a larger repulsive seed which prevents the particles from approaching closer for self-assembly. The morphologies generated by these particles are similar to an earlier work by Avvisati et. al³⁶. By varying a parameter l ($l = 2d/(\sigma_S + \sigma_L)$; d is the distance between the seed and the lobe, σ_S is the diameter of the seed and σ_L is the diameter of the lobe), they showed that snowman shaped particles (referred to as dumbbell shaped particles in their work) self-assemble into sheets at a higher l, spherical micelles at a lower l, and elongated micelles at a moderate l.

At a lower temperature ($k_BT=0.2$) dumbbell shaped particles self-assemble into a wide variety of structures at different seed di-

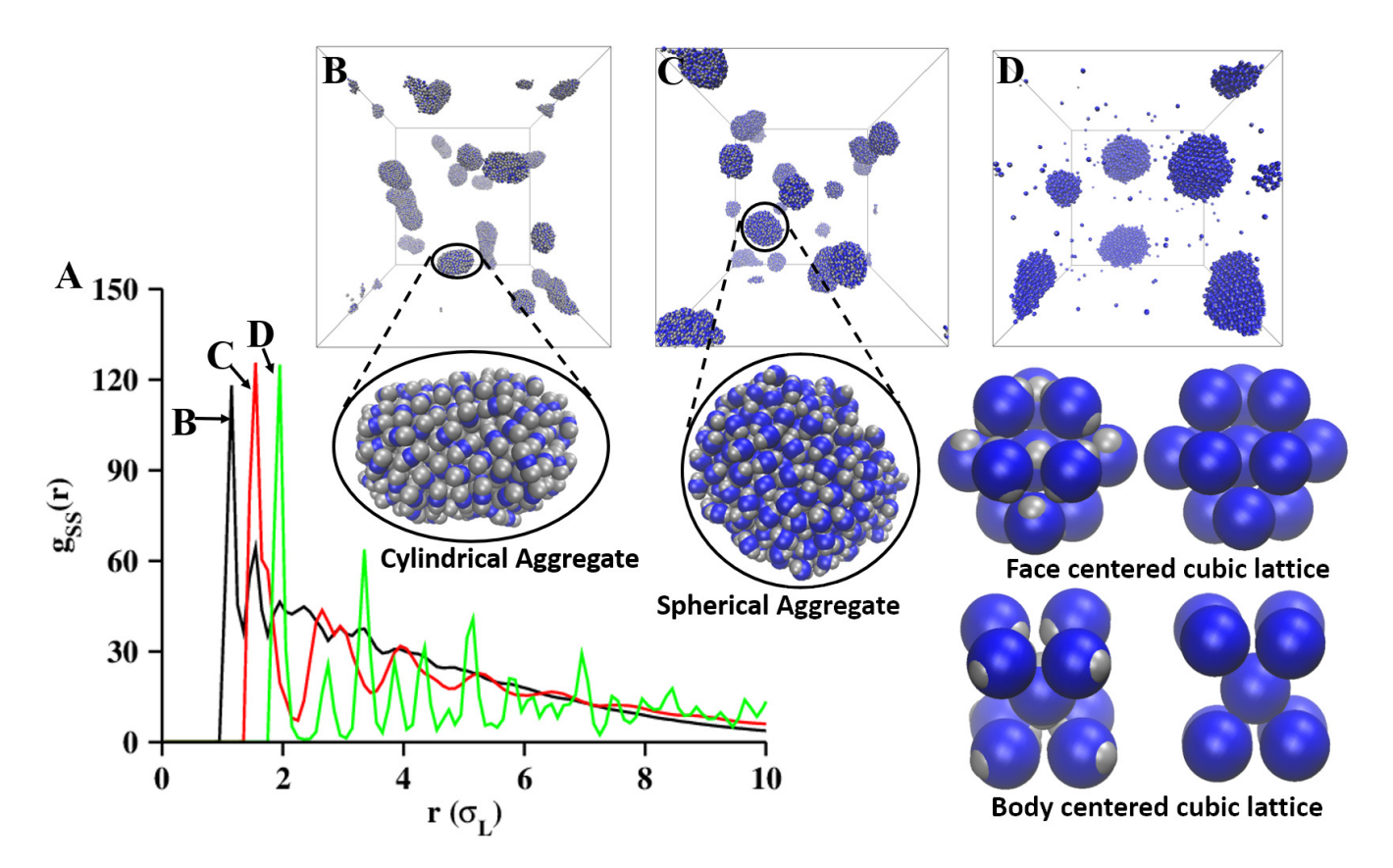


Fig. 3 Self-assembly of dumbbell shaped particles at $k_BT = 0.2$. (A) Radial distribution functions $[g_{SS}(r)]$ computed for the seed pairs at $k_BT = 0.2$ at three different seed diameters; $\sigma_S = 1.0$ (q = 1.0) (B), 1.4 (q = 0.71) (C) and 1.8 (q = 0.56) (D). Shown are simulation domains with (B) random aggregates of cylindrical shapes at $k_BT = 0.2$ and $\sigma_S = 1.0$, (C) spherical aggregates at $k_BT = 0.2$ and $\sigma_S = 1.4$; the enlarged views of the cylindrical and spherical aggregates are shown, and (D) crystalline structures at $k_BT = 0.2$ and $\sigma_S = 1.8$. Two different unit cells, face centered cubic and body centered cubic (with and without lobes) are also shown.

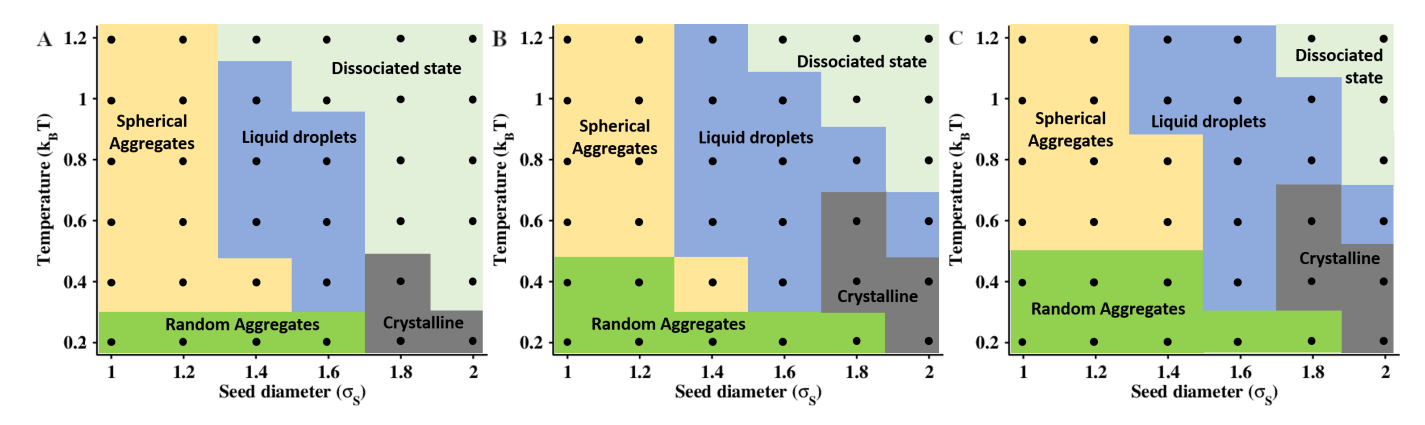


Fig. 4 Phase behavior of (A) trigonal planar, (B) square planar, and (C) tetrahedral lobed particles at different seed diameters and temperatures. The black dots show the exact locations of seed diameters and temperatures at which the self-assembly studies of the lobed particles were carried out.

ameters. When the seed diameter is smaller ($\sigma_S = 1.0$ or q = 1.0)₂₁₉ or lobes are larger, these particles self-assemble into random ag-220 gregates of cylindrical shapes, as confirmed by the RDF for the₂₂₁ seed-seed pairs where long range order is not present in these ag-222 gregates (Figs. 3A and 3B). When the seed diameter is increased₂₂₃ ($\sigma_S = 1.4$ or q = 0.71), the random aggregates are likely to attain₂₂₄ spherical shapes (Fig. 3C) and the seeds are more ordered which₂₂₅ is confirmed by the corresponding RDF. If the lobes are made very₂₂₆ small by increasing the seed size ($\sigma_S = 1.8$ or q = 0.56), dumb-227

bell particles self-assemble into crystalline structures (Fig. 3D). We find two different types of unit cells comprising these crystalline morphologies, face centered cubic and body centered cubic. At a higher temperature, dumbbell shaped particles mainly self-assemble into spherical aggregates irrespective of the seed or the lobe size. When seeds are smaller or lobes are larger, these aggregates are mainly random (Fig. S3A, ESI†), but if the seed diameter is increased, aggregates resemble liquid droplets showing that particles are ordered up to the second or third coordination

shells (Fig. S3B, ESI[†]).

229

230

232

233

234

235

236

237

238

239

240

241

242

243

244

246

247

248

249

250

251

252

253

254

255

256

257

258

260

261

262

263

264

265

266

267

268

269

270

271

272

273

274

275

276

277

278

279

281

282

For trigonal planar, square planar, and tetrahedral lobed par-285 ticles, we find a similar type of self-assembly behavior. For each286 type of particle, we identified four distinct self-assembled phases:287 random aggregates, spherical aggregates, liquid like droplets, and288 crystalline structures (Fig. 4). At lower temperatures, particles₂₈₉ self-assemble into random aggregates for a wide range of seed di-290 ameters (green regions in Fig. 4). Random aggregates appear in291 different shapes (e.g., cylindrical, wire like) and lack correlation292 between the particles present in them. With an increase in tem-293 perature, random aggregates are observed to undergo a transition294 to spherical aggregates (yellow regions in Fig. 4) at lower seed295 diameters, and to liquid droplets (blue regions in Fig. 4) at mod-296 erate seed diameters. For each type of particle, the transition from 297 random aggregates to liquid droplets happens along two different298 pathways depending on the seed diameter. At $\sigma_S = 1.4$ (q = 0.71),299 this transition is observed to occur via an intermediate phase com-300 prised of spherical aggregates, and at $\sigma_S = 1.6$ (q = 0.63), a direct₃₀₁ transition can occur from random aggregates to liquid droplets.302 At higher seed diameters, when lobes are very small, interactions303 between the particles become highly directional, and we observed 304 crystalline assembled structures at lower temperatures. We com-305 puted the number of particles (seeds) present in the first coordi-306 nation shells of the crystalline structures and found it to be 12 for307 all three types of lobed particles. For trigonal planar and tetra-308 hedral particles, the unit cell possess a hexagonal close packed309 geometry and for square planar particles, it is a face centered310 cubic. At higher seed diameters and higher temperatures, lobed311 particles appear in a dissociated state. In the case of trigonal312 planar particles, crystalline structures directly transitioned to dis-313 sociated state with an increase in temperature, and for square314 planar and tetrahedral lobed particles, this transition occurs via a315 liquid droplet phase. However, these transitions are found to oc-316 cur at different temperatures depending on the number of lobes317 and shapes of particles. For example, at $\sigma_S = 1.6$ (q = 0.63), trig-318 onal planar particles undergo a transition from the dissociated 319 state to a liquid droplet state when temperature is decreased to₃₂₀ 0.8 from 1.0. The same transition for the square planar particles₃₂₁ at the same seed diameter occurs upon decreasing the tempera-322 ture from 1.2 to 1.0. For tetrahedral lobed particles, this transi-323 tion occurs at a temperature higher than 1.2. These differences₃₂₄ in the transition temperatures, that arise due to differences in the325 number of lobes and the shapes of particles, are potentially use-326 ful to separate constituent lobed patchy particles from a mixture.327 The self-assembled morphologies and the corresponding RDFs for₃₂₈ these three types of particles are given in the supporting informa-329 tion (Fig. S4, S5 and S6, ESI[†]).

The morphologies of self-assembled structures presented so far331 were obtained at a low number density of particles ($\rho_N=0.008$).332 To understand the effect of particle density on the self-assembled333 structures, we carried out simulations for all five types of par-334 ticles at three higher densities ($\rho_N=0.016$, 0.037, 0.125) at a335 few selected seed diameters and temperatures. These simulations336 reveal that the self-assembled morphologies are independent of the particle density. For example, snowman shaped particles at 3388 $\sigma_S=1.0/q=1.0$ and at $k_BT=0.2$ form two-dimensional sheets at 339

three different higher densities (Fig. S7, ESI[†]). As expected, the size of each self-assembled structure is found to increase with an increase in ρ_N (Fig. S7 and S8, ESI[†]).

Porosity of self-assembled structures: We investigated porosities for those cases where larger three dimensional structures are formed through self-assembly. In that aspect, we ruled out the self-assembled structures formed by the snowman shaped particles, as these structures are either two dimensional sheets or micelles (Fig. 2). We computed pore size distributions (PSD) for the self-assembled structures obtained from the other four types of lobed particles using Zeo++ software ^{37,38}. We extracted large cuboids from assembled structures (Fig. S9, ESI[†]) and used those cuboids to determine the PSDs, which are given in the supporting information (Figs. S10, S11, S12, and S13, ESI[†]). For all types of lobed particles, we observed a similar trend in the variation of PSDs. At lower seed diameters and temperatures, pore diameters are very small ($\sim 0.1\sigma_L$) in random aggregates, and pore diameters are found to increase with an increase in temperature. At moderate seed diameters, distributions are broader at higher temperatures due to the formation of liquid droplets. For example, in the case of dumbbell shaped particles, pore diameters vary from $0.1\sigma_L$ to $2.3\sigma_L$ at $\sigma_S = 1.6$ (q = 0.63) and $k_BT = 0.4$ (Fig. S10D, ESI[†]). For tetrahedral lobed particles, at $\sigma_S = 1.6$ (q = 0.63) and $k_BT = 1.2$, pore diameters vary from $0.1\sigma_L$ to $1.6\sigma_L$ (Fig. S13D, ESI[†]). In the crystalline structures self-assembled at higher seed diameters and lower temperatures, pore diameters are uniform and we observed sharp peaks in the pore size distributions (Fig. S10E and S11F, ESI[†]). The pore diameters generated by the lobed particles are comparable to the diameter of the spherical beads (σ_L) that constitute the initial clusters. If we project our dimensionless simulations into real units, and if we choose 1 $\sigma_L = 1 \ \mu m$, then the porosities will vary from 0.1 μm to $2.3 \mu m$, depending on simulation conditions and the particle type. The largest pores, that we found in this study, are produced by the dumbbell shaped particles. The pore diameters for self-assembled structures formed by these particles are $\sim 2.3\sigma_L$.

In summary, by performing a series of Langevin dynamics simulations, we revealed how two crucial parameters, lobe size and temperature, control the morphologies, phases, and porosities of self-assembled structures generated by five different lobed patchy particles. We have introduced a modeling approach, which mimics a recently developed experimental method of synthesizing patchy particles 11, to model the lobed particles with different lobe sizes. Snowman shaped particles, which self-assemble only at a lower temperature, formed two-dimensional sheets, elongated and spherical micelles depending on the lobe size. Each of the other four types of particles (dumbbell, trigonal planar, square planar, and tetrahedral) was found to self-assemble into four distinct morphologies (random aggregates, spherical aggregates, liquid droplets, and crystalline) depending on the lobe size and temperature. At higher seed diameters (smaller lobes) and higher temperatures, these particles do not self-assemble and remain in a dissociated state. The self-assembled morphologies were found to be same at a range of particle densities. The transitions between any two specific phases occur at different temperatures for different lobed particles. This difference in the transition temper-

ature (mainly for the transition from a dissociated state to a con-405 densed phase) could be useful in separating a mixture of different 406 341 types of lobed particles. The self-assembled structures generated₄₀₈ 342 by these four types of particles are porous and their porosities are 409 found to depend on the lobe size and temperature. Pore diam-410 344 eters increase with an increase in temperature at any particular⁴¹² seed diameter. The largest pores were produced by the dumb-413 346 bell shaped particles. We suggest that porosities of self-assembled415 347 structures may be increased by increasing the repulsive interac-348 tions between seeds, possibly by including electrostatic interac-418 349 tions in future models. 350

Acknowledgements

We are grateful for financial support provided by the National 352 Science Foundation (award No. OIA-1757371; HV). We acknowl-353 edge computational support through the following resources: 354 Premise, a central shared HPC cluster at UNH supported by 355 the Research Computing Center; BioMade, a heterogeneous 356 CPU/GPU cluster supported by the NSF EPSCoR award (OIA-357 1757371; HV); and the NSF-supported (ACI-1548562) Extreme 358 Science and Engineering Discovery Environment (XSEDE) 39 359 Comet resource at San Diego Supercomputer Center (SDSC) un-360 der grant TG-MCB160183 (HV).

Conflicts of Interest

There are no conflicts to declare.

Notes and references

364

366

- 1 S. Ravaine and E. Duguet, Curr. Opin. Colloid Interface Sci, 2017, 30, 45–53.
 - 2 F. Li, D. P. Josephson and A. Stein, Angew. Chem. Int. Ed, 2011, 50, 360-388
- 367 3 S. C. Glotzer, M. J. Solomon and N. A. Kotov, AIChE Journal, 2004, 50, 2978–2985
- 368 4 Y. Xia, B. Gates and Z.-Y. Li, Adv. Mater., 2001, 13, 409–413.
- 369 5 A. B. Pawar and I. Kretzschmar, Macromol. Rapid Commun., 2010, 31, 150–168.
- M. Boncheva and G. M. Whitesides, in Biomimetic Approaches to the Design of Functional, Self Assembling Systems, ed. J. A. Schwarz, C. I. Contescu and K. Putyera, Marcel Dekker, Inc., New
 York, NY, First Edition edn, 2004, vol. 1, pp. 287–294.
- 373 7 Z. Zhang and S. C. Glotzer, Nano Lett., 2004, 4, 1407–1413.
- 374 8 Z. Zhang, A. S. Keys, T. Chen and S. C. Glotzer, Langmuir, 2005, 21, 11547–11551.
- 375 9 Q. Chen, S. C. Bae and S. Granick, Nature, 2011, 469, 381–384.
- D. J. Kraft, R. Ni, F. Smallenburg, M. Hermes, K. Yoon, D. A. Weitz, A. van Blaaderen, J. Groenewold, M. Dijkstra and W. K. Kegel, *Proc. Natl. Acad. Sci. U.S.A*, 2012, 109, 10787–10792.
- Y. Wang, Y. Wang, D. R. Breed, V. N. Manoharan, L. Feng, A. D. Hollingsworth, M. Weck and
 D. J. Pine, *Nature*, 2012, 491, 51–55.
- 380 12 K. H. Ku, Y. Kim, G.-R. Yi, Y. S. Jung and B. J. Kim, ACS Nano, 2015, 9, 11333–11341.
- J. A. Diaz A., J. S. Oh, G.-R. Yi and D. J. Pine, Proc. Natl. Acad. Sci. U.S.A, 2020, 117, 10645–
 10653.
- 383 14 I. C. Pons-Siepermann and S. C. Glotzer, ACS Nano, 2012, 6, 3919–3924.
- 384~15~ A. W. Long and A. L. Ferguson, Mol. Syst. Des. Eng. , 2018, $\boldsymbol{3},$ 49–65.
- 385 16 A. W. Long and A. L. Ferguson, J. Phys. Chem. B, 2014, 118, 4228–4244.
- 386 17 D. Morphew, J. Shaw, C. Avins and D. Chakrabarti, ACS Nano, 2018, 12, 2355–2364.
- 387 18 T. S. Skelhon, Y. Chen and S. A. F. Bon, Soft Matter, 2014, 10, 7730-7735.
- 19 A. Tsyrenova, K. Miller, J. Yan, E. Olson, S. M. Anthony and S. Jiang, *Langmuir*, 2019, 35,
 6106–6111.
- D. J. Kraft, W. S. Vlug, C. M. van Kats, A. van Blaaderen, A. Imhof and W. K. Kegel, J. Am.
 Chem. Soc., 2009, 131, 1182–1186.
- 392 21 L. Hong, A. Cacciuto, E. Luijten and S. Granick, *Langmuir*, 2008, **24**, 621–625.
- B. Bharti, D. Rutkowski, K. Han, A. U. Kumar, C. K. Hall and O. D. Velev, J. Am. Chem. Soc,
 2016, 138, 14948–14953.
- 395 23 J. S. Oh, S. Lee, S. C. Glotzer, Y. Gi-Ra and D. J. Pine, Nat. Commun, 2019, 10, 3936.
- 396 24 A. W. Wilber, J. P. K. Doye and A. A. Louis, J. Chem. Phys., 2009, 131, 175101.
- 25 A. Giacometti, F. Lado, J. Largo, G. Pastore and F. Sciortino, J. Chem. Phys., 2010, 132,
 174110.
- 26 F. Liu, S. Goyal, M. Forrester, T. Ma, K. Miller, Y. Mansoorieh, J. Henjum, L. Zhou, E. Cochran
 and S. Jiang, *Nano Lett.*, 2019, 19, 1587–1594.
- 401 27 V. N. Manoharan, M. T. Elsesser and D. J. Pine, Science, 2003, 301, 483–487.
- 402 28 S. Paul and H. Vashisth, Soft Matter, 2020, 16, 1142-1147.
- 403 29 Q. L. Loh and C. Choong, Tissue Eng. Part B Rev., 2013, 19, 485-502.
- 04 30 J. B. Matson, R. H. Zha and S. I. Stupp, Curr. Opin. Solid State Mater. Sci., 2011, 15, 225–235

- 31 S. Sacanna, M. Korpics, K. Rodriguez, L. Colón-Meléndez, S.-H. Kim, D. J. Pine and G.-R. Yi, Nat. Commun, 2013, 4, 1688.
- 32 Z. Gong, T. Hueckel, G.-R. Yi and S. Sacanna, Nature, 2017, 550, 234-238.
- 33 V. Meester, R. W. Verweij, C. van der Wel and D. J. Kraft, ACS Nano, 2016, 10, 4322-4329.
- 34 J. A. Anderson, C. D. Lorenz and A. Travesset, J. Comp. Phys., 2008, 227, 5342-5359.
- 35 J. Glaser, T. D. Nguyen, J. A. Anderson, P. Lui, F. Spiga, J. A. Millan, D. C. Morse and S. C. Glotzer, Comput. Phys. Commun, 2015, 192, 97–107.
- 36 G. Avvisati, T. Vissers and M. Dijkstra, J. Chem. Phys., 2015, 142, 084905.
- 37 M. Pinheiro, R. L. Martin, C. H. Rycroft and M. Haranczyk, CrystEngComm, 2013, 15, 7531-7538.
- 38 M. Pinheiro, R. L. Martin, C. H. Rycroft, A. Jones, E. Iglesia and M. Haranczyk, J. Mol. Graph. Model, 2013, 44, 208–219.
- 39 J. Towns, T. Cockerill, M. Dahan, I. Foster, K. Gaither, A. Grimshaw, V. Hazlewood, S. Lathrop, D. Lifka, G. D. Peterson, R. Roskies, J. R. Scott and N. Wilkins-Diehr, *Comput. Sci. Eng.*, 2014, 16, 62–74.